scientific reports

Check for updates

OPEN

Evaluation of intra-fractional CBCT image quality using different megavoltage beam sizes and imaging conditions in a phantom study

Ruining Song✉, Shumin Cui & Baomin Chen

The intra-fractional cone beam computed tomography can provide real-time anatomical information while saving treatment time, leading to important breakthroughs in image-guided radiation therapy. However, MV-level photon scattering during the image acquisition will disrupt the image quality. We obtained intra-fractional cone beam computed tomography images of a standard phantom using different sizes of MV-beam and imaging conditions such as imaging time, tube current and tube voltage. We analyzed the uniformity index, noise power spectrum, low contrast visibility and spatial resolution of the images to investigate the effect of MV-level photon scattering on the image quality of intra-fractional cone beam computed tomography. It was found that these parameters of the images varied regularly with the size of the MV-beam, which can help us to predict in advance whether the quality of the images meets the clinical requirements based on the radiation treatment plan to decide whether to use intra-fractional cone beam computed tomography. The research also shows that the different imaging conditions can improve or deteriorate the image parameter, which can also help us choose reasonable imaging conditions to obtain better image quality according to the clinical situation.

Keywords Intra-fractional cone beam computed tomography, Scattering, Uniformity index, Noise power spectrum, Low contrast visibility, Spatial resolution

Image-guided radiation therapy is acknowledged to be a major advancement in radiation therapy that has improved precision and accuracy in positioning. This development leads to increased tumor control probability and decreased normal tissue complication probability. As the cornerstone technology of image-guide radiation therapy (IGRT), cone-beam computer tomography (CBCT) is widely used to assess organ motion and dose administration in thoracic and abdominal tumors, particularly in techniques such as volumetric modulated arc therapy and adaptive radiotherapy[1–4].

In addition to reducing the overall treatment time, intra-fractional CBCT can provide real-time anatomical information during the treatment[5,6]. Nevertheless, few studies have focused on how MV-level photon scattering can compromise the quality of intra-fractional CBCT images. W Luo et al. highlighted that the MV-level photon scattering significantly diminished the target visibility in the kV image, which could be enhanced by modifying the imaging parameters[7]. Georgia Friend et al. investigated the effect of MV filed size on intra-fractional CBCT images, noting a decline in image quality with increasing field size[8]. Kim et al. also found that the contrast-to-noise ratio dropped from 6.3 to 2.6 because of the MV-level photon scattering and the intra-fractional CBCT image quality was also affected by the tube current and monitor units of the treatment plan[9]. Yoganathan et al. discovered that the accuracy of Hounsfield Units (HU), Contrast-to-Noise Ratio (CNR) and Signal-to-Noise Ratio (SNU) were affected by MV-level scattering, and this effect became more pronounced with larger beam sizes and lower photon energy[10]. Williams et al. demonstrated the contrast detail decreased with MV-beam, resulting in increased image noise and a noticeable loss of bony anatomy detail[11]. To improve the image quality of intra-fractional CBCT, M. van Herk et al. proposed a correction method based on alternating pulse sequences[12]. Ouyang et al. installed a constantly moving physical attenuator made of equal-spaced strips of lead between the CBCT source and the patient to improve image quality based on constraint optimization[13]. Despite ongoing

Department of radiotherapy, Shanxi Provincial People's Hospital, Shuangtasi Street No.29, Taiyuan 030012, China. ✉email: songruining0729@outlook.com

interest in MV-level photon scattering since the advent of intra-fractional CBCT, a comprehensive analysis of the image quality using a standard test phantom remains absent.

This paper aims to analyze how MV-level photon scattering affects the image quality of the intra-fractional CBCT. The research investigates the effects across different MV-beam field sizes and imaging conditions of intra-fractional CBCT using the Catphan phantom. Based on the results of this study, clinicians can make informed decisions about whether to use intra-fractional CBCT and select the most appropriate imaging preset parameters for achieving the best image quality.

Results

Uniformity

The experiment results indicated that UI remained approximately 14% when the length of the square beam fields ranged from 1 cm to 5 cm. It increased linearly (slope = 0.51) from 14.44 to 22.27% as the length of the square MV-beam increased from 5 cm to 20 cm. For the reference CBCT with no MV-beam, maintained a UI of 0.84%, as shown in Fig. 1a. In Fig. 1b, with changes in the imaging time, UI remained constantly around 8% with the 10 cm×10 cm MV-beam and increased slightly but little overall change with no MV-beam. When the tube current increased from 10 mA to 80 mA, UI increased linearly (slope = 0.101) from 9.44 to 15.77% with the 10 cm×10 cm MV-beam and had a similar linear (slope = 0.105) increase with no MV-beam, as displayed in Fig. 1c. An increase in tube voltage from 70 kV to 140 kV resulted in an exponential decrease in UI from 20.1% to almost zero with the 10 cm×10 cm MV-beam, UI without MV-beam decreased between tube voltage of 70 kV and 90 kV and then remained almost constant, as shown in Fig. 1d.

Figure 2a shows that the lines connecting CT values along the horizontal and vertical diameter were similar. The curvature of these lines intensified with larger beam fields, indicating a more pronounced cupping artifact. As Fig. 2b showed, minimal changes in these curves of the cupping artifact were observed for different imaging times with the 10 cm×10 cm MV-beam. Without the MV-beam, the lines connecting CT values became more flexural with longer imaging time. In Fig. 2c, the curvature of the curves increased with higher tube currents, both with and without the MV-beam. The higher tube voltage weakened the cupping artifact and even eliminated it with 130 kV and 140 kV with the 10 cm×10 cm MV-beam. The connecting lines remained flatter without MV-beam as shown in Fig. 2d. Figure 2b, c indicated that longer imaging time and higher tube current resulted in greater edge hardening.

To analyze the pattern of the cupping artifact with different beam fields, nonlinear curve-fitting using Eq. (1) on the CT value connecting lines could be employed. All datasets were fitted successfully, and the fitting results

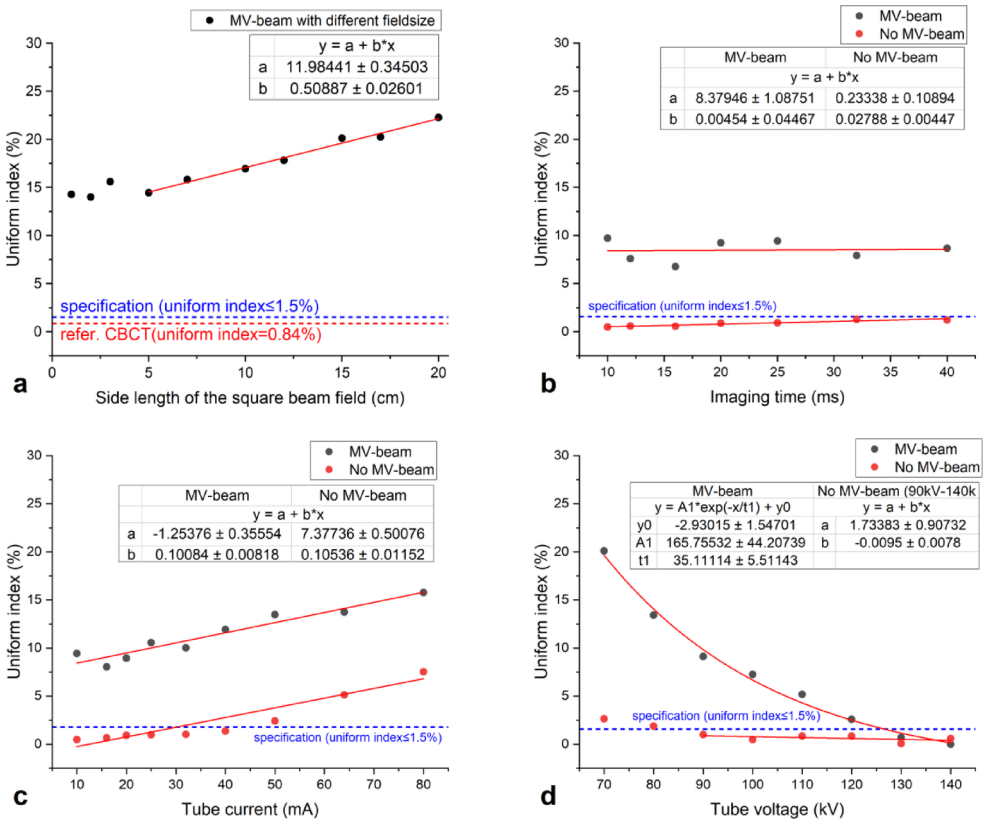

Fig. 1. The uniformity index of different side lengths of the square beam field (**a**); imaging times (**b**); tube current (**c**), tube voltages (**d**).

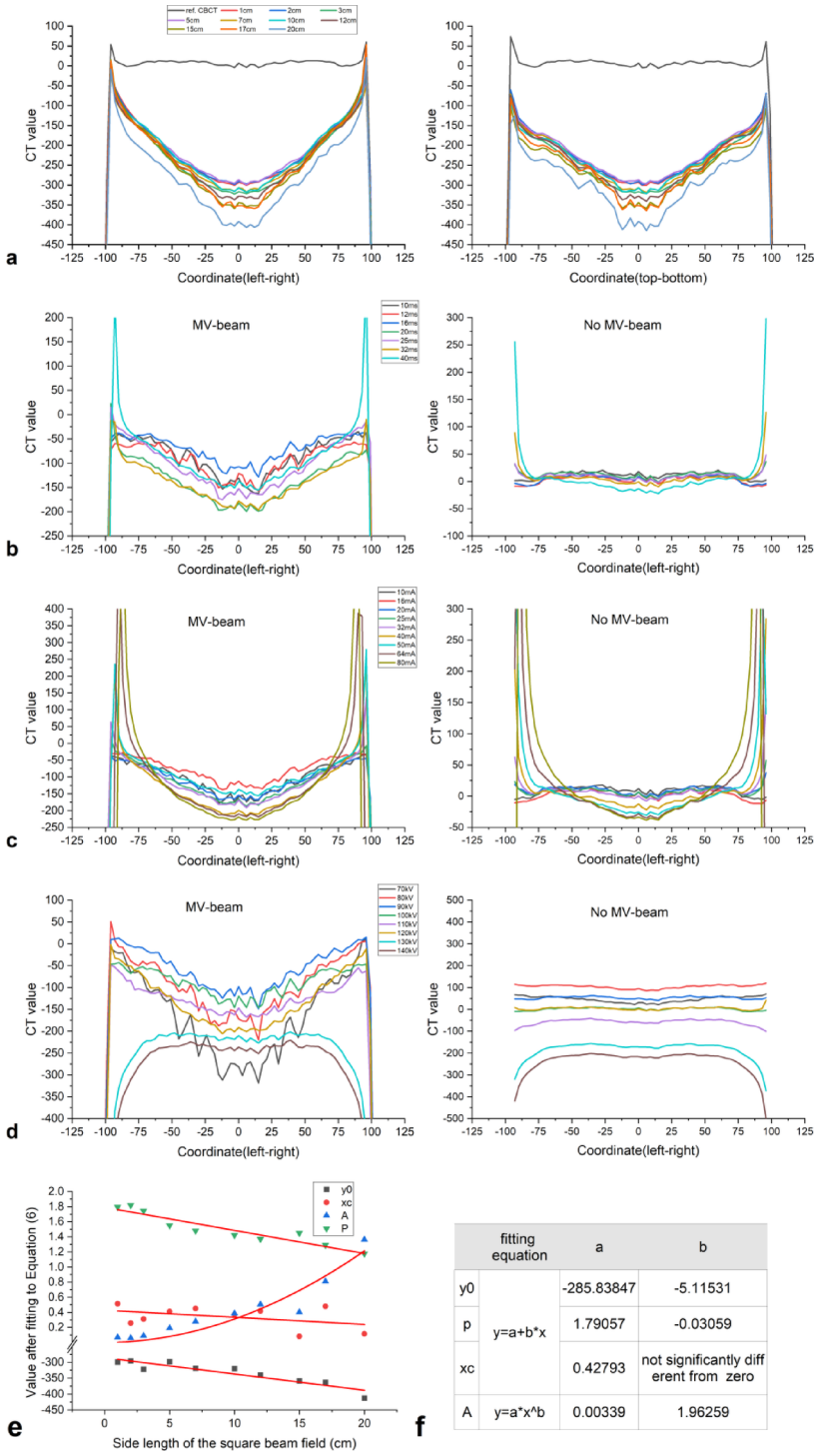

	fitting equation	a	b
y0	y=a+b*x	-285.83847	-5.11531
p		1.79057	-0.03059
xc		0.42793	not significantly diff erent from zero
A	y=a*x^b	0.00339	1.96259

Fig. 2. (**a**) The CT value of the small circle measured along the horizontal diameter (left: left to right) and the vertical diameter (right: top to bottom) under different side lengths of square beam fields; the CT value of the small circle measured along the horizontal diameter (left: left to right) with and without the MV-beam with different imaging times (**b**), tube currents (**c**), tube voltages (**d**); (**e**) fitting results of the CT value connection lines along horizontal diameter for different side lengths of square beam fields by Eq. (1); (**f**) the fitting results of the four parameters of Eq. (1).

for y_0, p and A were shown in Fig. 2e, whereas the fitted results for x_c consistently hovered around zero. Only the horizontal cupping artifacts were fitted, because the horizontal and vertical curves exhibited similarity.

$$y = y_0 + A|x - x_c|^p \tag{1}$$

Figure 2e showed that with an increased beam field, the coefficients of Eq. (1) y_0 and p changed linearly and could be fitted by $y = a + bx$, whereas A changed exponentially and could be fitted by $y = ax^b$. The fitting results were presented in Fig. 2f.

Noise power spectrum

For better comparison, we normalized both iNPS and NSD to the minimum value observed in each group's experiment. NPS for all four groups exhibited a peak at the same spatial frequency between 0.05 and 0.1 mm^{-1}. With an increased MV-beam field, the intensity of NPS increased, and the normalized iNPS also increased but the normalized NSD showed minimal variation, as shown in Fig. 3a.

In Fig. 3b, c, d, the intensity of NPS with 10 cm×10 cm MV-beam decreased significantly with an increase in the imaging time, tube current, and tube voltage, leading to a corresponding decrease in the normalized iNPS. As a reference, i.e. without the MV-beam, the intensity of NPS only had a slight decrease, which can also be seen in the changes in iNPS. The normalized NSD without MV-beam is subject to changes in imaging conditions differently than it is subject to changes in MV-beam field size. As the imaging time increased, with and without the MV-beam, the NSD decreased initially and then remained almost constant after 16 ms. For the increased tube current, the NSD with the 10 cm×10 cm MV-beam decreased and remained constant after 25 mA, but the NSD first declined and then increased when there was no MV-beam. Higher tube voltage significantly decreased the NSD significantly with the 10 cm×10 cm MV-beam and had little impact for the no MV-beam scenario.

Low contrast visibility

In Fig. 4a, LCV of the reference CBCT with no MV-beam was 0.69%. With a small MV-beam field, LCV remained approximately 1% and initiated a linear increase (slope = 0.17) from 1.12 to 3.46% as the length of the square beam field extended from 5 cm to 20 cm. In Fig. 4b, as the imaging time increased from 10 ms to 40 ms, LCV decreased linearly (slope=−0.08) from 3.82 to 1.55% with 10 cm×10 cm MV-beam and decreased slightly linearly (slope=−0.01) without MV-beam. With 10 cm×10 cm MV-beam LCV underwent an exponential decrease from 7.29 to 1.42% with an increased tube current from 10 mA to 80 mA, and stayed nearly the same without MV-beam, as shown in Fig. 4c. Furthermore, with 10 cm×10 cm MV-beam, LCV decreased linearly (slope=−0.22) from 13.24 to 2.28% with an increased tube voltage from 70 kV to 120 kV and remained almost constant when the tube voltage exceeded 120 kV, meanwhile LCV decreased slightly linearly without the MV-beam, as illustrated in Fig. 4d.

The Spatial resolution

In Fig. 5a, it was evident that the spatial resolution decreased as the 6MV-beam field increased. With the 10 cm×10 cm MV-beam, longer imaging time and higher tube current and tube voltage improved the spatial resolution, as shown in Fig. 5b, c, d and the improvement from each increase in ms, mA, and kV were slight. In the absence of the MV-beam, the impact on spatial resolution at different imaging times was negligible, but higher tube current and tube voltage could also improve the spatial resolution.

Discussion

To the best of our knowledge, this study is the most detailed investigation to date of intra-fractional CBCT image quality. Instead of the simulation model, which can only be used to subjectively evaluate image quality, it delved into the effect of MV-level photon scattering on kV-level CBCT using a standard phantom for CT image analysis. The study meticulously examined the uniformity, artifact, NPS, LCV, and spatial resolution of the intra-fractional CBCT image using MV-beam fields of different sizes. Additionally, we analyzed the effects of different CBCT imaging conditions, such as imaging time, tube current, and tube voltage, on image quality while maintaining a fixed-size MV-beam. The results of this study hold the potential to anticipate image quality and guide the selection of optimal imaging parameters for obtaining higher-quality images.

With the 6MV photon scattering, all aspects of the intra-fractional CBCT image performance degrade with the increased beam field, in line with the prior studies[7–9,14]. Even with a beam as small as 1 cm×1 cm, UI becomes significantly higher than in the reference CBCT without MV-beam. The linear increase in UI with the MV-beam field indicates that the deterioration can be predicted, corresponding to the predictable cupping artifacts, the main reason for the uniformity disruption. This insight hints that inverse processing of the image based on the predicted cupping artifacts might improve uniformity.

The intensity of NPS and iNPS also increase with an increased MV-beam field size, indicating that more scattering from a larger MV-beam field generates more noise in the image. The work by W Luo and Kim noted that an increase in MV-beam field size can lower the contrast-to-noise ratio, which is consistent with the conclusion about image noise with the larger MV-beam field size[7,9] On the other hand, NSD shows minimal variation with a larger beam field, suggesting that NSD may not be an ideal representation of the noise level.

LCV increases as the MV-beam field size increases, which is consistent with the findings in Friend's paper[8],. However, LCV remains within the specification (≤ 3%) until the MV-beam field size exceeds 18 cm×18 cm. This means that LCV of the intra-fractional CBCT image satisfies the requirements in most instances with 25 ms, 40 mA and 120 kV, the imaging conditions of the first group experiment listed in Table 1. On the other hand, MTF, representing the spatial resolution, noticeably worsens with an increased MV-beam field size. According to Eq. (6), the main factors influencing the MTF include the standard deviations of the uniform region of the

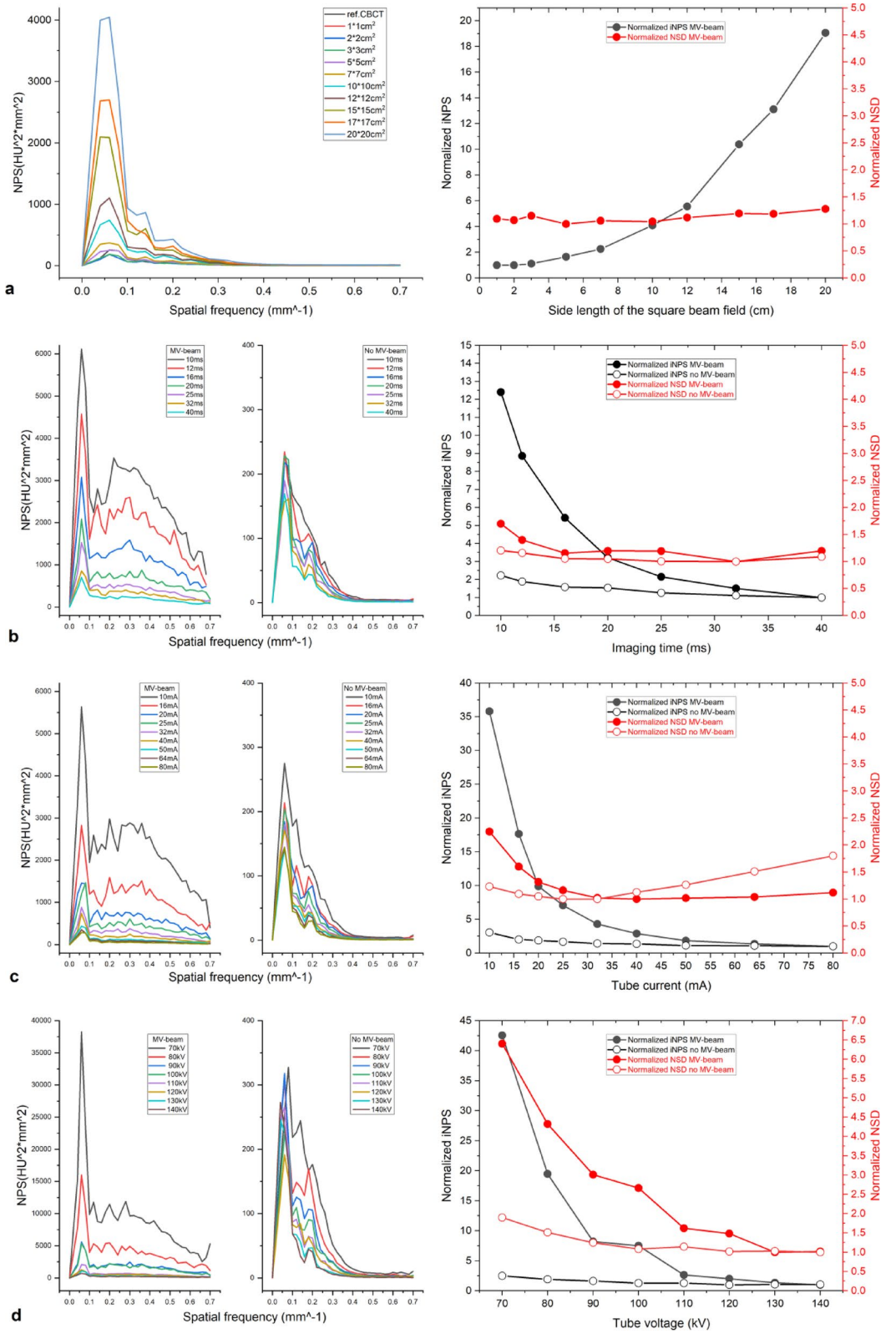

Fig. 3. The noise power spectrum (NPS), the normalized integrated noise power spectrum (iNPS) and the normalized noise standard deviation (NSD) with the different side lengths of the square beam fields (**a**), imaging times (**b**), tube currents (**c**), tube voltages (**d**).

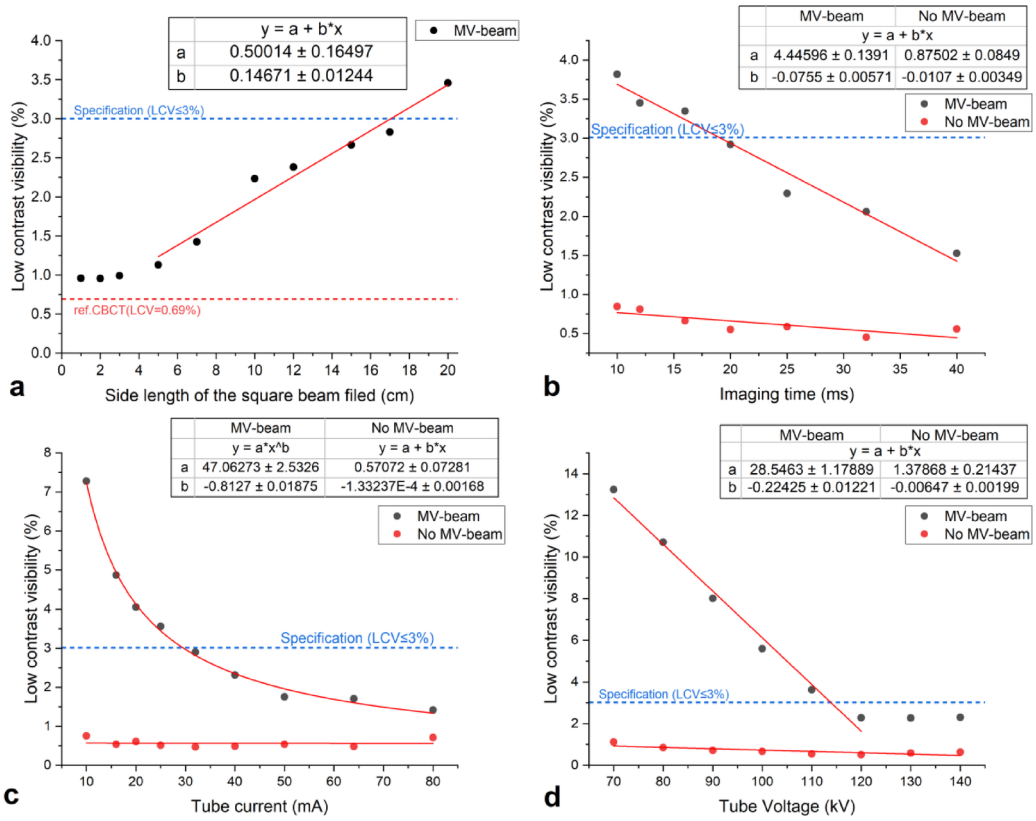

Fig. 4. Low contrast visibility under different side lengths of the square beam fields (**a**), imaging times (**b**), tube currents (**c**), tube voltages (**d**).

phantom, the aluminum slice, and the rectangular area that encompasses each line pair. A larger MV-beam field introducing more scattering increased the standard deviation for the materials, which resulting in more severe degradation of the intra-fractional CBCT image quality for anatomical sites with high-density materials like bones. This may also explain the higher failure rate for registration of the intra-fractional CBCT for the anatomical tumor in Friend's paper[8].

With a longer imaging time, although there is a slight increase in UI and the cupping artifacts in the absence of MV-beam, the effect is negligible compared to the effect of MV-beam on UI and the cupping artifacts. Thus, UI and the cupping artifacts remain essentially unchanged with longer imaging time when the MV-beam is present. Without the MV-beam, longer imaging time can slightly optimize LCV and noise but has a slight improvement on spatial resolution. However, with the MV-beam, longer imaging time can improve noise, LCV and spatial resolution, providing less improvement for NSD than for NPS and LCV. Caution is necessary as longer imaging time with a high dose rate may lead to more scattering. Given the limited research focus on the effect of imaging time, future research could delve into this aspect in greater detail.

For the tube current, it is notable that without the MV-beam, a higher tube current elevates UI linearly, with the slope of this increase being almost equal to that in the presence of an MV-beam. This indicates that the change in the tube current does not affect the uniformity destruction due to the MV-level scattering, and that the increase in the tube current itself leads to a deterioration of the uniformity. Without the MV-beam, higher tube current slightly reduces NPS while decreasing and then increasing the NSD, but the overall change in noise is not particularly large. In the presence of MV-beam, a higher tube current is very beneficial for NPS, NSD, LCV and spatial resolution. It is noteworthy that a higher tube current can improve the image quality in terms of noise and LCV, aligning with the literature by Kim[9]. However, the negative effect on UI should also be considered.

The experiments show that increasing the tube voltage is the most effective way to improve the image quality of the intra-fractional CBCT. Unlike the slight improvement seen without the MV-beam, a higher tube voltage significantly enhances image quality in the presence of an MV-beam. With increased tube voltage, the cupping artifacts are mitigated and even eliminated when the tube voltage reaches 130 kV and 140 kV, bringing UI very close to that of the reference CBCT. This indicated that the hardening of the kV rays by MV-level scattering no longer produced the cupping artifacts at 130 kV and 140 kV, leading to a notable improvement in image uniformity. In future studies, we can investigate whether the hardening of 130 kV and 140 kV rays due to the MV-level scattering of higher MV-beam will lead to the appearance of the cupping artifacts. NPS, NSD, LCV, and spatial resolution all exhibit improvement for the intra-fractional CBCT. Further research is necessary to establish the correlation between the energy of the MV-beam and the tube voltage eliminating the cupping artifacts.

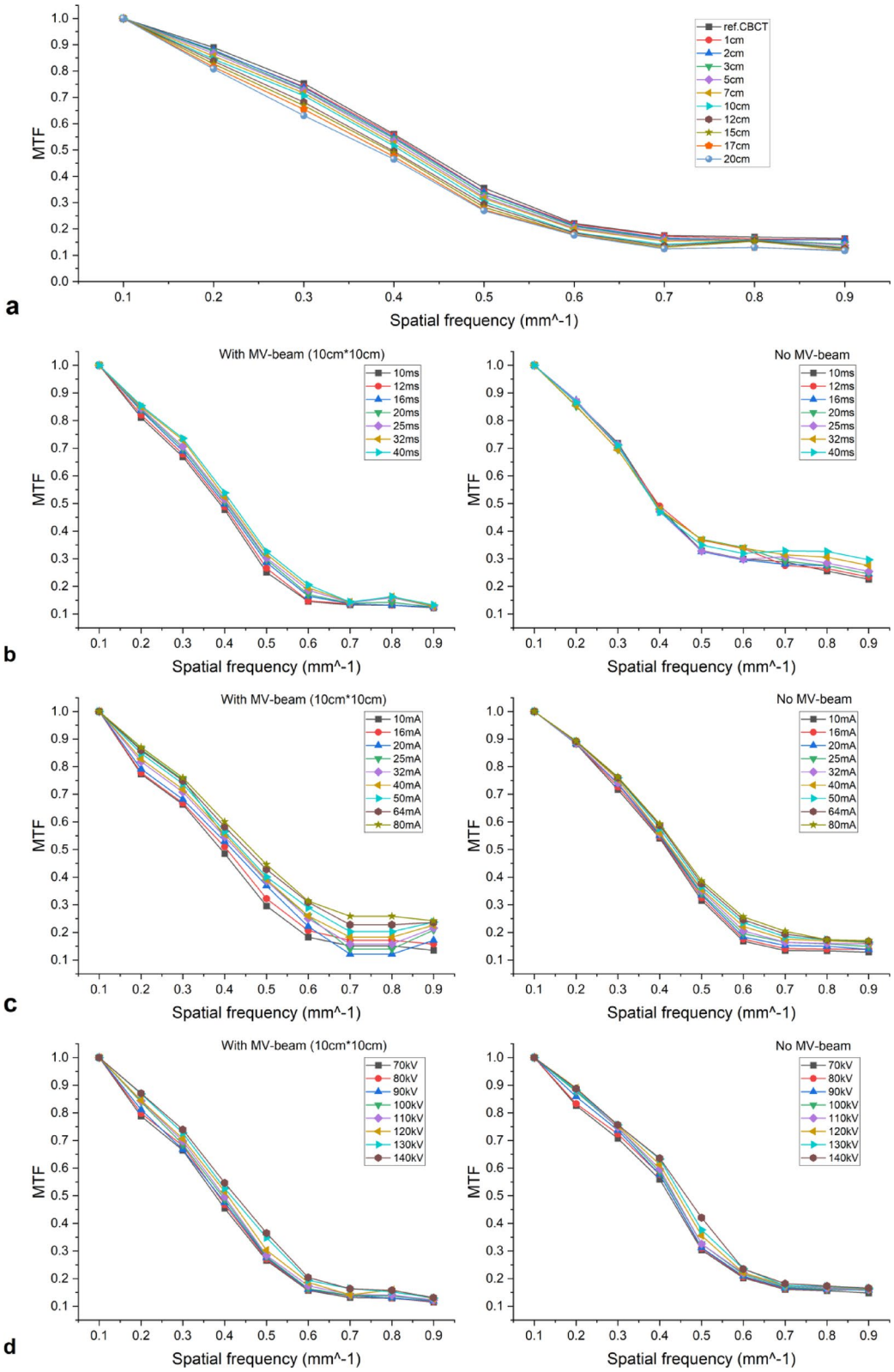

Fig. 5. Modulation Transfer Function (MTF) under different side lengths of the square beam fields (**a**), imaging times (**b**), tube currents (**c**), tube voltages (**d**).

Stationary parameters for all experiments	MV-beam		kV-CBCT	
	Delivery	3D ARC with 6MV	kV-collimator	S10
	Total monitor unit (MU)	600	kV-filter	F0
	Dose rate (MU/min)	600	Frames	330
	Gantry rotation		360° (−180°→180°, clockwise)	
	Gantry speed (°/s)		6°/s	
The variable parameters and stationary parameters for the four groups experiments	Variable parameters		Stationary parameters	
	MV-beam size (cm×cm)	0(reference), 1 × 1, 2 × 2, 3 × 3, 5 × 5, 7 × 7,10 × 10, 12 × 12, 15 × 15, 17 × 17, 20 × 20	Imaging time per frame (ms)	25
			Tube current (mA)	40
			Tube voltage (kV)	120
	Imaging time per frame (ms)	10, 12, 16, 20, 25, 32, 40	MV-beam size (cm×cm)	10 × 10, 0(reference)
			Tube current (mA)	40
			Tube voltage (kV)	120
	Tube current (mA)	10, 16, 20, 25, 32, 40, 50, 64, 80	MV-beam size	10 × 10, 0(reference)
			Imaging time per frame (ms)	40
			Tube voltage (kV)	120
	Tube voltage (kV)	70, 80, 90, 100, 110, 120, 130, 140	MV-beam size (cm×cm)	10 × 10, 0(reference)
			Imaging time per frame (ms)	25
			Tube current (mA)	40

Table 1. MV-beam field sizes and imaging conditions of CBCT used in the experiments.

It is important to keep in mind that constantly increasing the imaging time, tube current, and tube voltage does not necessarily lead to improved image quality. In reality, it may even be detrimental to the image quality and increase the heat generated by the CBCT tube. Therefore, selecting suitable imaging conditions should consider the anatomical structure and clinical requirements. According to the experimental results of this study, higher tube voltage can significantly improve all parameters of the image quality. Increasing tube current and lengthening the imaging time are completely ineffective when uniformity is important, but for improving LCV and noise, especially NPS, both can be very effective. For better spatial resolution, longer imaging time, higher tube current and voltage are available as a good option. Although our investigation had similar results to the existing literature[7–11], we still need to conduct studies on more accelerators to enhance the applicability of the findings in this study.

This study aims to investigate the effects of different MV-beam field sizes, imaging time, tube current, and tube voltage of CBCT on the image quality of intra-fractional CBCT. The utilization of a standard phantom can enhance the quantification of the effects, a critical aspect currently absent in the research area of intra-fractional CBCT images. The study has unveiled the patterns in the effects of beam field size and imaging conditions on image quality, providing valuable support for clinicians to predict image quality and select the most reasonable imaging conditions for the intra-fractional CBCT.

Methods

Phantoms and image acquisition

In this study, our experimental framework was based on the published report of AAPM[15], Bissonnette et al.'s paper[16], and Elekta's XVI test manual. Our focus was on critical factors such as uniformity, noise power spectrum (NPS), low contrast visibility (LCV), and spatial resolution. The experimentation was conducted using the Elekta Infinity accelerator, featuring the Agility collimator and intra-fractional CBCT functionality.

To ensure meticulous image analysis, we utilized the Catphan phantom (The Phantom Laboratory, Greenwich, NY, Fig. 6f). The phantom comprises multiple modules designed for diverse parameter evaluations. For uniformity and noise measurements, we employed Module CTP 486 which is made of water-equivalent uniform material. We used Module CTP 515, including eight cylindrical rods made of different materials, to measure LCV. The spatial resolution test involved Module CTP 528, incorporating 21 aluminum line pairs with varying thicknesses. Evaluating the specific parameters of CBCT objectively is the main reason we chose the Catphan phantom.

We used ImageJ[17], a program developed by the National Institutes of Health, to analyze the image data and OriginPro (Version 2021, OriginLab Corporation, Northampton, MA, USA.). for mathematical processing.

The image acquisition process was divided into four groups, each corresponding to a different variant. The beam fields were set as square fields with different side lengths from 1 cm to 20 cm, and the imaging conditions were set as 25 ms, 40 mA and 120 kV because they are the most common imaging conditions for inter-fractional CBCT and are also set in the on-board presets for intra-fractional CBCT. We set different imaging times, tube currents and tube voltage with a 10 cm×10 cm MV-beam and no MV-beam as reference to investigate the effect of the imaging conditions on the intra-fractional CBCT. The imaging conditions were determined based on the hardware constraints of the accelerator and Elekta's XVI test manual, with spacing non-constant and limited

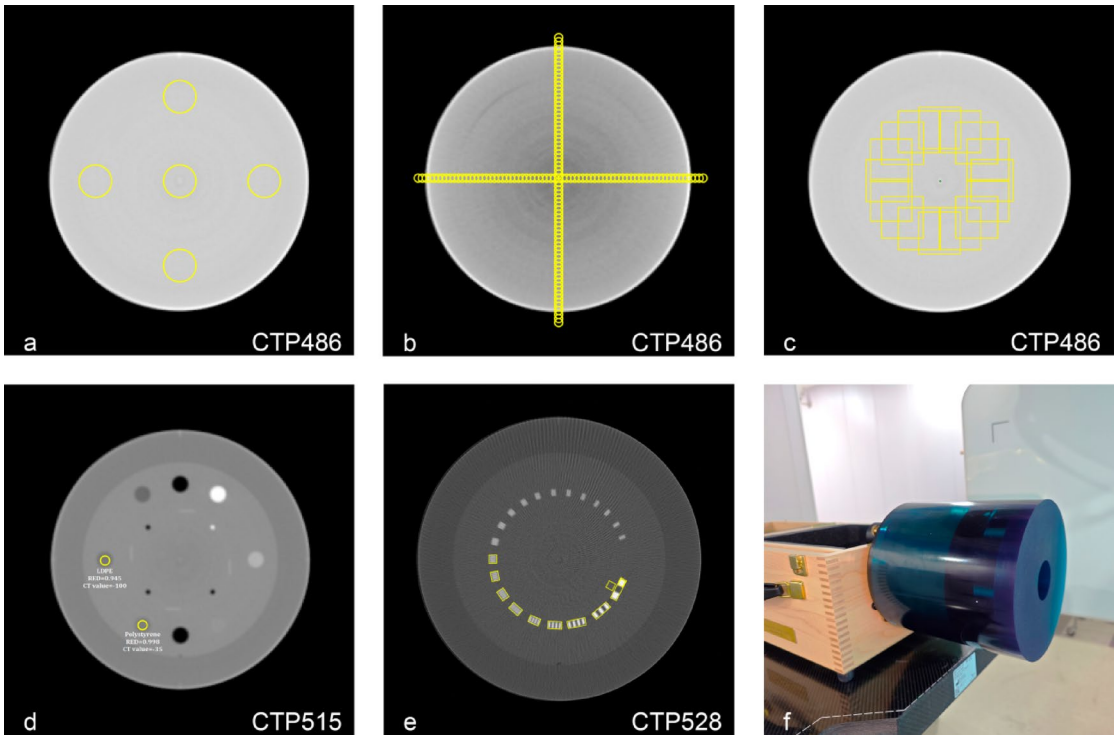

Fig. 6. Regions of interest to evaluate the performance of image quality: (**a**) five circle regions to calculate uniformity index; (**b**) small circles with a diameter of 3 mm along the horizontal and vertical diameters to assess cupping artifact; (**c**) 16 square regions to calculate the noise power spectrum; (**d**) the mean CT value and standard deviation of low-density polyethylene and polystyrene to evaluate low contrast visibility; (**e**) rectangular regions for the Modulation Transfer Function calculation; (**f**) the photo of the Catphan phantom.

to specific values. The frames of the intra-fractional CBCT was 330 for the 360° scanning for 1 min, which means the scanning speed is constantly 5.5 frames/s. The energy of the MV-beam was 6MV, which is the most commonly utilized energy in radiation therapy and is suitable for nearly all sites of tumor. To accurately assess the impact of MV-level scattering on intra-fractional CBCT image quality, we maintained a constant dose rate of 600MU/min, the highest dose rate available on our accelerator. This constant dose rate ensured that the intra-fractional CBCT experienced stable MV-level scattering. The specific parameter settings are listed in Table 1.

Notably, experiments within each group, focusing on one module of the Catphan phantom were conducted concurrently to mitigate the effects of temperature, humidity, and air pressure on the accelerator's output dose and the intra-fractional CBCT imaging. There was no correction for the scattering during the reconstruction and analysis of the CBCT image and the image at the isocenter was chosen to analyze the image quality.

Uniformity

Uniformity refers to the consistency of pixel values on the CBCT image when scanning a uniformly attenuated object. A higher uniformity index (UI) indicates a greater level of nonuniformity and thus potentially worse image quality. The calculation method[16,18] involved taking five regions of the same size in the image of CTP486, encompassing one at the center and four at the periphery, as shown in Fig. 6a. UI was calculated by Eq. (2):

$$UI = 100 \cdot (CT\#_{max} - CT\#_{center}) / CT\#_{center} \quad (2)$$

where $CT\#_{max}$ is the maximum value of the mean CT values of the four peripheral regions and $CT\#_{center}$ is the mean CT value of the central region.

The cupping artifacts are manifested as a decrease in value from the periphery toward the center of the figure in the reconstructed image, which is mainly due to beam hardening and scattering. Using a flat and large-area detector in CBCT increases sensitivity to scattering, which can cause cupping artifacts and significantly affects the uniformity of the intra-fractional CBCT image[19]. The specific manifestation of the cupping artifacts can be observed in Fig. 6b. The CT value of the uniform equivalent water phantom Catphan CTP486 gradually decreases from the periphery to the center. We measured the mean CT value of the small circle regions along the horizontal and vertical diameters of the phantom to assess the cupping artifact, as shown in Fig. 6b.

Noise power spectrum

NPS provides a comprehensive depiction of noise. It characterizes the texture of noise by representing the variance of noise as a function of spatial frequency. The Wiener spectrum[20], also known as NPS, is the Fourier

transform of the autocorrelation function, which describes noise correlation in the spatial domain. The 2D NPS is expressed as[21]

$$NPS\left(f_x, f_y\right) = \sum_{1}^{N} \left|\mathrm{DFT}_{2\mathrm{D}}\left(I_i\left(x,y\right) - \bar{I}_i\right)\right|^2 \cdot \left(\Delta_x \Delta_y\right) / \left(N_x N_y\right) \cdot N^{-1} \tag{3}$$

where $I_i\left(x,y\right)$ is the signal in the ith region of interest ROI and $\bar{I}_i$ is the mean of $I_i\left(x,y\right)$. Δ corresponds to the pixel spacing in a given plane. N_x, N_y are the number of voxels and f_x, f_y are the spatial frequencies in each dimension of the ROI. $\mathrm{DFT}_{2\mathrm{D}}$ is the discrete Fourier transform in 2D. The summation over I and multiplicated by N^{-1} refers to averaging the NPS over N ROIs, and f_x, f_y in 2D NPS can be collapsed to a 1D radial frequency, f_r as

$$f_r = \sqrt{f_x^2 + f_y^2} \tag{4}$$

To calculate the final NPS, we averaged the NPS of the 16 square regions located 40 mm from the center, as shown in Fig. 6c. An integrated NPS (iNPS) was also calculated over the entire frequency range to describe the intensity of NPS, which also can be compared to the average noise standard deviation (NSD).

Low contrast visibility

LCV refers to the ability of a system to distinguish materials with minimal differences in absorption coefficients. It was determined by measuring the mean CT value of two materials, Polystyrene and Low-Density Polyethylene (LDPE), as illustrated in Fig. 6d, and was calculated using Eq. (5) from the XVI customer acceptance test manual:

$$low\ contrast\ visibility = 6.5 / \left(\left(\bar{x}_{poly} - \bar{x}_{LDPE}\right) / \left(\left(\sigma_{\ poly} + \sigma_{\ LDPE}\right)/2\right)\right) \tag{5}$$

where 6.5 is the constant difference between the CT values of the polystyrene and LDPE, $\bar{x}_{poly}$ and $\bar{x}_{LDPE}$ are the mean CT values and $\sigma_{\ poly}$ and $\sigma_{\ LDPE}$ are the standard deviations of the polystyrene and LDPE. A lower value calculated by Eq. (5) means more easier to distinguish different materials, i.e., a better image quality.

The Spatial resolution

The Modulation Transfer Function (MTF), calculated using the Droege-Morin method[22], was used to assess the spatial resolution. MTF was tested on Module CTP528 which consisted of aluminum slices with different widths separated by specific gap widths. The Droege-Morin formula for MTF calculation is given by:

$$MTF\left(f\right) = \pi\sqrt{2} \cdot M\left(f\right)/4M_0 \tag{6}$$

$$M\left(f\right) = \sqrt{SD_{linepair}^2 - SD^2},\ SD^2 = \left(SD_{Al}^2 + SD_{water}^2\right)/2,\ M_0 = \left|CT\#_{Al} - CT\#_{water}\right|/2.$$

where SD_{water}, SD_{Al} and $SD_{linepair}$ are the standard deviation (SD) of the uniform region of the phantom, the aluminum slice and a rectangular region that includes each line pair. The measurement regions are set up as Fig. 6e. The spatial frequency $f = (N-1)/10$ in cycles/mm of the rectangular regions is associated with the number of line pairs.

Data availability

The datasets generated during and/or analysed during the current study are available from the corresponding author on reasonable request.

Received: 20 June 2024; Accepted: 2 May 2025
Published online: 08 May 2025

References

1. Hattu, D. et al. A traffic light protocol workflow for image-guided adaptive radiotherapy in lung cancer patients. *Radiother. Oncol.* **175**, 152–158 (2022).
2. Posiewnik, M. & Piotrowski, T. A review of cone-beam CT applications for adaptive radiotherapy of prostate cancer. *Physica Med.* **59**, 13–21 (2019).
3. De Jong, R. et al. Feasibility of conebeam CT-based online adaptive radiotherapy for neoadjuvant treatment of rectal cancer. *Radiat. Oncol.* **16**, 136 (2021).
4. Van Timmeren, J. E. et al. Treatment plan quality during online adaptive re-planning. *Radiat. Oncol.* **15**, 203 (2020).
5. Li, W. et al. The use of cone beam computed tomography for image guided gamma knife stereotactic radiosurgery: initial clinical evaluation. *Int. J. Radiation Oncology*Biology*Physics*. **96**, 214–220 (2016).
6. Zeng, L. et al. Analysis of the amplitude changes and baseline shifts of respiratory motion using intra-fractional CBCT in liver stereotactic body radiation therapy. *Physica Med.* **93**, 52–58 (2022).
7. Luo, W., Yoo, S., Wu, Q. J., Wang, Z. & Yin, F. F. Analysis of image quality for real-time target tracking using simultaneous kV-MV imaging: simultaneous kV-MV imaging. *Med. Phys.* **35**, 5501–5509 (2008).
8. Friend, G., O'Connor, P. & Charles, P. The effect of megavoltage field size on intrafraction cone-beam CT image quality. *Phys. Eng. Sci. Med.* **43**, 711–717 (2020).
9. Kim, J. et al. Image quality of 4D in-treatment CBCT acquired during lung SBRT using FFF beam: a Phantom study. *Radiat. Oncol.* **15**, 224 (2020).

10. Yoganathan, S. A. et al. Evaluating the image quality of cone beam CT acquired during rotational delivery. *BJR* **88**, 20150425 (2015).
11. Williams, P., Sykes, J. & Moore, C. The effects of radiation scatter from simultaneous MV irradiation on KV fluoroscopic and X-ray volume imaging with the Elekta synergy system. *Radiother. Oncol.* **73**, S229–S230 (2004).
12. Van Herk, M., Ploeger, L. & Sonke, J. J. A novel method for megavoltage scatter correction in cone-beam CT acquired concurrent with rotational irradiation. *Radiother. Oncol.* **100**, 365–369 (2011).
13. Ouyang, L., Lee, H. P. & Wang, J. A moving blocker-based strategy for simultaneous megavoltage and kilovoltage scatter correction in cone-beam computed tomography image acquired during volumetric modulated Arc therapy. *Radiother. Oncol.* **115**, 425–430 (2015).
14. Ling, C. et al. Acquisition of MV-scatter-free kilovoltage CBCT images during RapidArc™ or VMAT. *Radiother. Oncol.* **100**, 145–149 (2011).
15. Klein, E. E. et al. Task group 142 report: quality assurance of medical acceleratorsa). *Med. Phys.* **36**, 4197–4212 (2009).
16. Bissonnette, J. P., Moseley, D. J. & Jaffray, D. A. A quality assurance program for image quality of cone-beam CT guidance in radiation therapy: image quality QA of cone-beam CT. *Med. Phys.* **35**, 1807–1815 (2008).
17. Schneider, C. A., Rasband, W. S. & Eliceiri, K. W. NIH image to imageJ: 25 years of image analysis. *Nat. Methods*. **9**, 671–675 (2012).
18. Nakahara, S., Tachibana, M. & Watanabe, Y. One-year analysis of Elekta CBCT image quality using NPS and MTF. *J. Appl. Clin. Med. Phys.* **17**, 211–222 (2016).
19. Xie, S., Li, C., Li, H. & Ge, Q. A level set method for cupping artifact correction in cone-beam CT: A level set method for cupping artifact correction. *Med. Phys.* **42**, 4888–4895 (2015).
20. Faulkner, K. & Moores, B. M. Analysis of x-ray computed tomography images using the noise power spectrum and autocorrelation function. *Phys. Med. Biol.* **29**, 1343–1352 (1984).
21. Boone, J. M. et al. Report 87. *Journal of the ICRU* 12, NP-NP (2012).
22. Droege, R. T. & Morin, R. L. A practical method to measure the MTF of CT scanners. *Med. Phys.* **9**, 758–760 (1982).

Author contributions

RS designed and performed the study, analyzed the data, and wrote the manuscript. SC and BC assisted with the experiment and data analysis.

Declarations

Competing interests

The authors declare no competing interests.

Additional information

Correspondence and requests for materials should be addressed to R.S.

Reprints and permissions information is available at www.nature.com/reprints.

Publisher's note Springer Nature remains neutral with regard to jurisdictional claims in published maps and institutional affiliations.